JKAU: Eng. Sci., **vol. 13 no. 1,** pp.47-68 (1421 A.H. / 2001 A.D.)

On Power Requirements of an Articulated Robotic Arm

A.N.N. Aljawi, M. Akyurt, H. Diken,
H. Bogis and F.M. Dehlawi
Faculty of Engineering, King Abdulaziz University,
Jeddah, Saudi Arabia

Abstract. Angular velocity and torque requirements of an articulated robotic arm, comprising an assembly of three links and three revolute joints, are considered. To ascertain the influence of link lengths on angular velocity requirements, kinematic relationships are established, and velocity-orientation surfaces are presented for selected tip speeds. Furthermore, general expressions are presented for determining torque requirements at the joints of the arm. The results are applied to a selected set of robot and motion specifications.

Key words: *Acceleration, angle, arm, force, joint, link, manipulator, mass, robot, torque, velocity.*

1. Introduction

Robots and robotic systems are synthesized from a number of interrelated and interacting subsystems which characterize the entire facility with respect to its flexibility and applicability to a certain task. These subsystems for a robot typically include a manipulator, gripper, power sources, drives, control systems, sensory systems, computer and/or micro-processors, and the necessary software. The present industrial robots are actually mechanical handling devices that are manipulated under computer control.

Of the several hundred different designs of robots in existence currently, about 95% are in the form of fixed-base arms (manipulators), and are used in materials handling operations and, in some cases, doing such jobs as welding and painting. These are the so-called *industrial robots.* The great majority of these do not possess a sense of touch or force feedback. They are programmed to do a certain task repetitively, and they do this at high speed (up to 1.5 m/s and 240 deg/s), and with high accuracy (up to ± 0.02 mm)[1].

Robotic *manipulators* or industrial robots comprise essentially an *arm* and a *wrist.* The arm consists of a series of binary mechanical links attached by joints. The joints in an arm are used to control the relative motion between its links. An arm typically has three joints or three degrees of freedom. Like in the human arm, the wrist is located at the most distal point of the arm, and consists of a group of joints. A typical wrist has three degrees of freedom, and provides motions of roll, pitch and yaw. Robotic manipulators generally possess six degrees of freedom, although industrial robots with three, four and five degrees of freedom also exist. The number of degrees of freedom of the wrist are reduced in those applications where less than six degrees of freedom are required.

Structurally robots can be classified as Cartesian, cylindrical, spherical and articulated robots according to the type of joints utilized on the arm. Denoting a linear joint by *P* (prismatic) and a rotary joint by *R*, the above classification may be alternately referred as a) PPP, b) PPR, c) PRR, and d) RRR. Each of these types has applications where it is best suited.

One of the most important performance characteristics of an arm is the shape of its *reach envelope* or *work space.* The shape of the work depends on the joint structure of the arm, and its size depends on the dimensions of its links. It is to be noted that the work space specified by the manufacturer will be exceeded when a gripper or a tool is attached to the wrist.

Articulated robots feature an arm that consists of three rigid members connected by two revolute joints. The arm itself is mounted on a rotary base (Fig. 1). The kinematic arrangement resembles the human arm. The gripper is analogous to the human hand, being attached to the forearm via a wrist.

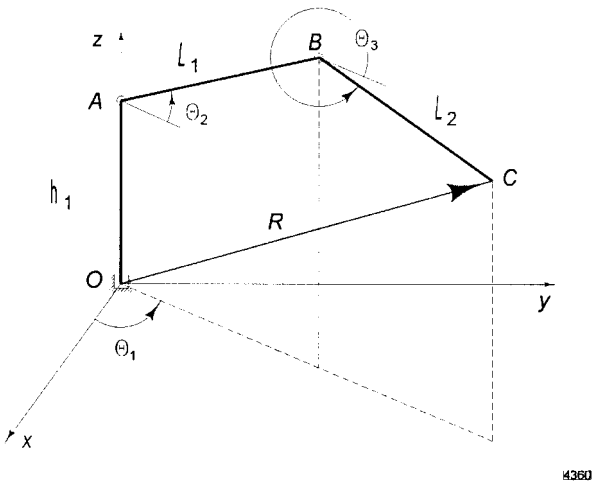

FIG. 1. Schematic view of the arm.

Due to the presence of three revolute joints, the resolution is the articulated robot depends on the configuration of the arm. The accuracy is relatively poor since errors at the joints are accumulated at the end effector. As for its advantages, the articulated robot can move at high speeds. Perhaps the most significant characteristic of the articulated robot is its excellent mechanical flexibility. It is perhaps because of these advantages that the articulated robots are the most common of all small and medium sized robots. The work envelope forms a major portion of a sphere.

Mannaa, Dehlawi and Akyurt[2] discussed geometric design considerations for a 3-link articulated robot arm. Raghavan and associates[3] described the design procedure for the manipulator and gripper of a robot comprising two revolute joints, at the shoulder and the elbow, and a prismatic joint at the gripper. The revolute joints were actuated by stepper motors, while the gripper was pneumatically operated. Herbest[4] discussed the trade-off process while designing a robot for a specific application.

Kim[5] proposed a design methodology to design an optimal manipulator for a given task. To this end he decomposed the task into the steps of kinematic design, planning, and kinematic control, using optimization at each step. A number of other studies were conducted on various aspects of the design of robots[6-11].

In what follows, we consider a three-link arm, as shown in Fig. 1, with three revolute joints. Since power is the product of torque and angular velocity, we investigate angular velocities as well as torque requirements at the joints of the arm.

2. Investigation of Angular Velocities

It would be interesting to investigate the angular velocities required to achieve a given target tip speed at various configurations of the arm. The value of 1.0 m/s seems to be a favored tip speed[11]. To this end, consider the position vector **R** in Fig. 1.

$$\mathbf{R} = h_1\,\mathbf{k} + L_1 \sin\Theta_2\,\mathbf{k} + L_1 \cos\Theta_2\,(\sin\Theta_1,\,\mathbf{j} + \cos\Theta_1\,\mathbf{i}) + L_2 \sin\Theta_3\,\mathbf{k} + L_2 \cos\Theta_3\,(\sin\Theta_1\,\mathbf{j} + \cos\Theta_1\,\mathbf{i})$$

Letting $\mathbf{r} = \mathbf{R} / L_1$, one obtains the normalized form of **R**:

$$\mathbf{r} = c\,[\,\cos Q_1\,\mathbf{i} + \sin Q_1\,\mathbf{j}\,] + [\,a + d\,]\,\mathbf{k} \qquad (1)$$

where $a = h_1 / L_1$

$b = L_2 / L_1$

$$c = \cos \Theta_2 + b \cos \Theta_3$$
$$d = \sin \Theta_2 + b \sin \Theta_3$$

A weighted velocity $\dot{\mathbf{r}} = \mathbf{V_c} / L_1$ of point C in Fig. 1 can be obtained by the differentiation of Eq. (1) with respect to time.

$$\begin{aligned}\dot{\mathbf{r}} = \mathbf{i} [&- \omega_2 \sin \theta_2 \cos \theta_1 - \omega_1 \sin \theta_1 \cos \theta_2 - b\omega_3 \sin \theta_3 \cos \theta_1 - b\omega_1 \\ &\sin \theta_1 \cos \theta_3] + \mathbf{j} [- \omega_2 \sin \theta_2 \sin \theta_1 + \omega_1 \cos \theta_1 \cos \theta_2 - b\omega_3 \sin \theta_3 \\ &\sin \theta_1 + b\omega_1 \cos \theta_1 \cos \theta_3] + \mathbf{k} [\omega_2 \cos \theta_2 + b\omega_3 \cos \theta_3] \end{aligned} \quad (2)$$

Now several cases can be identified.

Case 1: Vanishing ω_2 and ω_3 (θ_2 and θ_3 are kept constant)

For this case Eq. (2) takes the form

$$\mathbf{r} = \omega_1 c [- \sin \theta_1 \mathbf{i} + \cos \theta_1 \mathbf{j}]$$

For a magnitude of unity for $\dot{\mathbf{r}}$, it may be shown that

$$\omega_1 = \frac{1}{\cos \theta_1 + b \cos \theta_3} \quad (3)$$

Figures 2a to 2c display the variation of ω_1 with Θ_2 and Θ_3 for several values of b. It may be verified from these figures that the magnitude of ω_1 remains less than 2 rad/s over much of the robot, *i.e.,* $-70 < \Theta_2 < 70^\circ$ and $-115 < \Theta_3 < 170^\circ$. The magnitude of the angular velocity about the z-axis needs to be higher, however, at the "corners" of the domain, *i.e.,* when the absolute value of Θ_3 exceeds about 1.6 radians and Θ_2 exceeds about 1.0 radian when $b = 0.3$ (Fig. 2a). These regions correspond to the "folded up" configurations of the robot. Moreover, when b is increased to 0.7 (Fig. 2b) and to 1.2 (Fig. 2c), the ranges of $\Theta_2$and Θ_3, within which ω_1 is confined to 2 rad/s, become more restricted near the folded-up configurations.

Case 2: Vanishing ω_1 and ω_3

Equation 2 simplifies to

$$\dot{\mathbf{r}} = \omega_2 d[-\cos \theta_1 \mathbf{i} - \sin \theta_1 \mathbf{j} + \frac{c}{d} \mathbf{k}]$$

When the magnitude of $\dot{\mathbf{r}}$ is set to unity, it may be shown that

$$\omega_2 = \frac{1}{\sqrt{c^2 + d^2}} \quad (4)$$

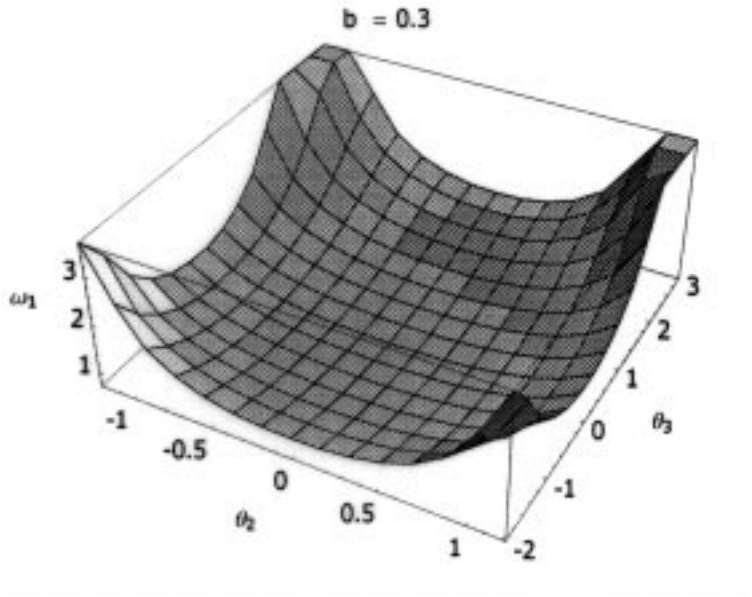
b = 0.3
ω_1
3
2
1
-1
-0.5
0
0.5
1
θ_2
-2
-1
0
1
2
3
θ_3

FIG. 2(a)

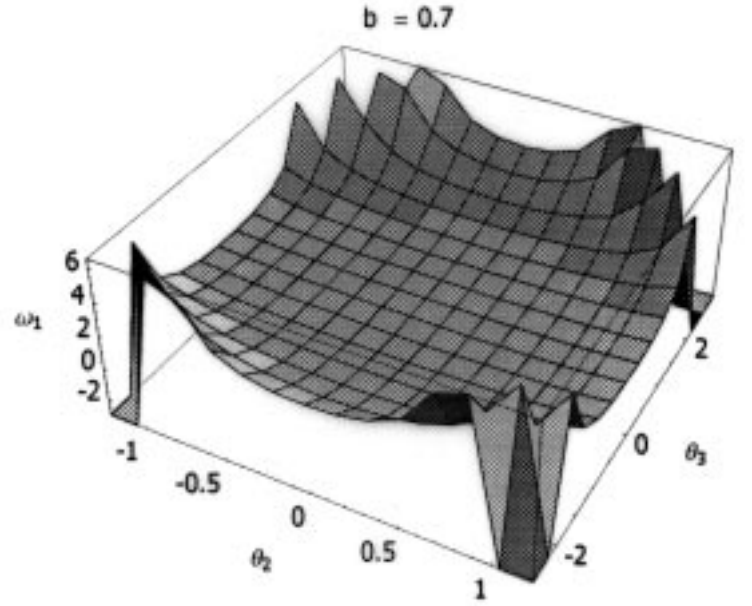
b = 0.7
ω_1
6
4
2
0
-2
-1
-0.5
0
0.5
1
θ_2
-2
0
2
θ_3

FIG. 2(b)

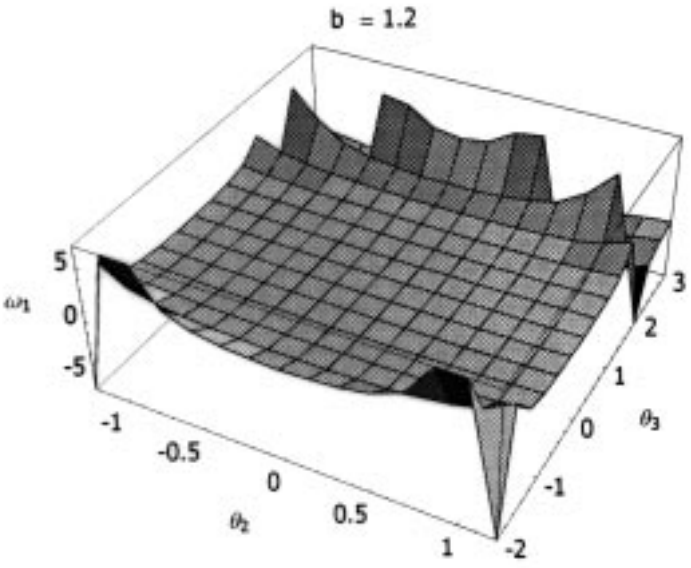

FIG. 2(c)

FIG. 2. Variation of ω_1 with θ_2 and θ_3.

It is to be noted for this case that ω_2 and ω_3 are identical.

Figures 3a to 3c depict the variation ω_2 with Θ_2 and Θ_3 for selected values of *b*. It may observed from these figures that the magnitude of ω_2 remains below 1 rad/s over a wide range of operation of the robot. The angular velocity of L_1 needs to be further increased, however, in some regions. These regions comprise the two diagonally opposing corners of the graphs where the absolute value of Θ_3 exceeds about 2 radians (120 degrees). At these locations, the arm is in the folded position, with L_1 nearly vertical. The rise in ω_2 is moderate when b = 0.3 (Fig. 3a), and it becomes more pronounced for b = 0.7 (Fig. 3b) and for b = 1.2 (Fig. 3c).

Case 3: Vanishing ω_1 and ω_2

For this Eq. (2) simplifies to

$$\dot{\mathbf{r}} = -b\omega_3 [\sin \theta_3 \cos \theta_1 \ \mathbf{i} + \sin \theta_3 \sin \theta_1 \mathbf{j} - \cos \theta_3 \mathbf{k}]$$

When the magnitude of $\dot{\mathbf{r}}$ is set to unity, it may be readily shown that this expression yields

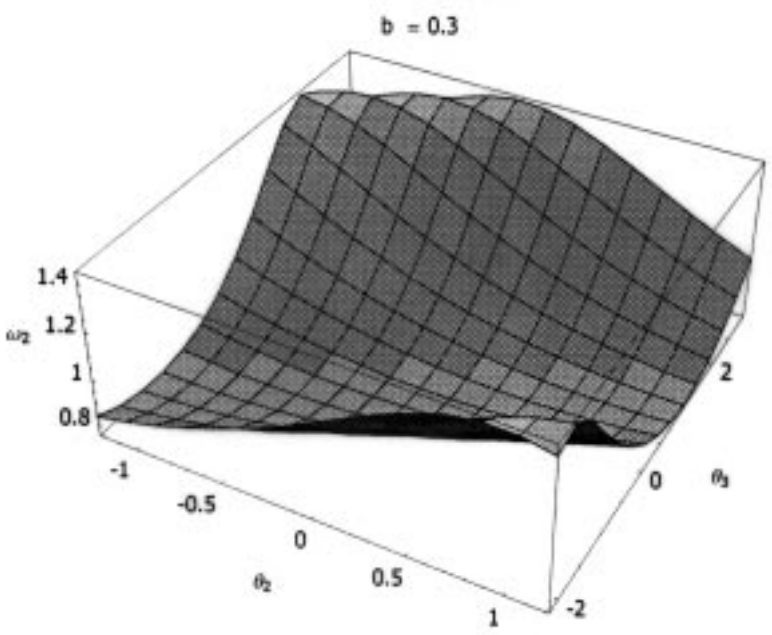

FIG. 3(a)

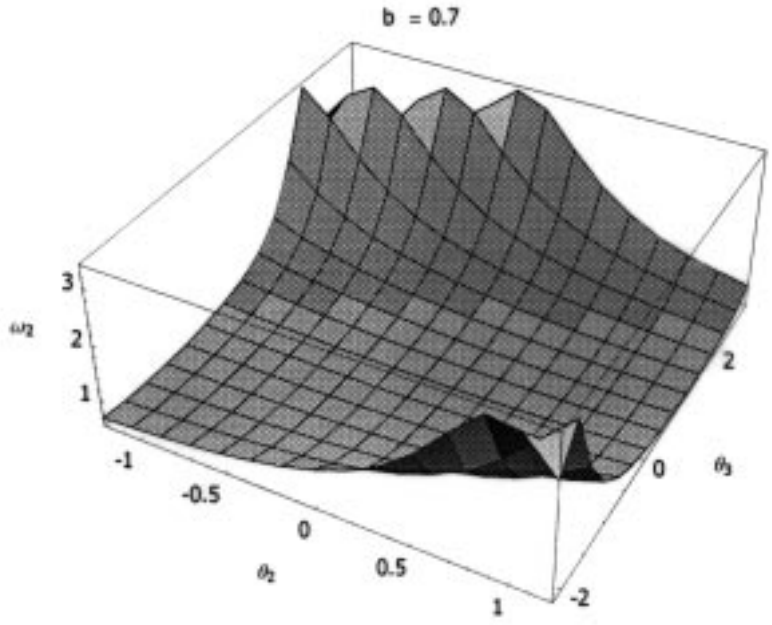

FIG. 3(b)

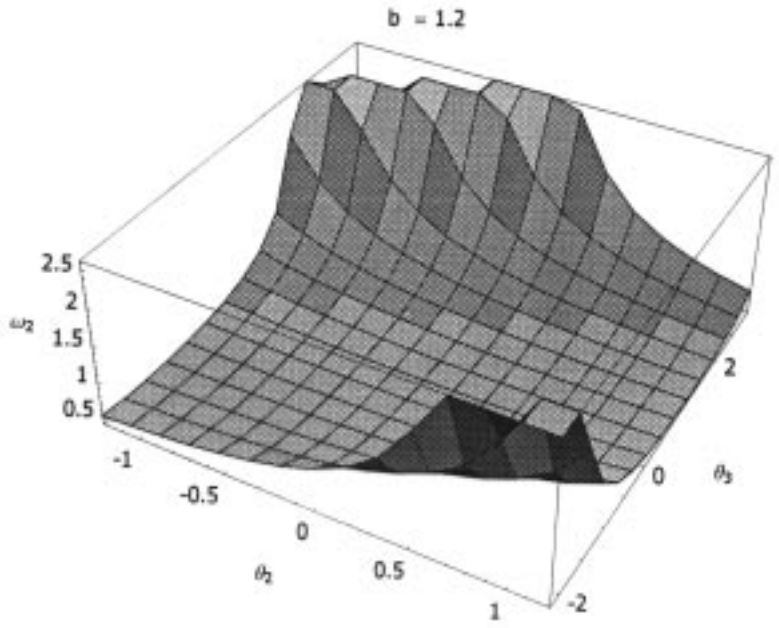

FIG. 3(c)

FIG. 3. Variation of ω_2 with θ_2 and θ_3.

$$\omega_3 = \frac{1}{b} \tag{5}$$

where $b = L_1 / L_2$. Thus ω_3 equals 3.3, 1.4 and 0.8 rad/s when b is set equal to 0.3, 0.7 and 1.2, respectively.

In summary of the above discussion, it may be concluded that angular velocities in the three-link arm tend to remain below 3 rad/s for a weighted tip velocity of unity per second. Magnitudes of the required angular velocities are dependent on *b,* generally growing with it.

3. Investigation of Torque Requirements

The dynamic equation at joint *i* of a manipulator may be stated as

$$\frac{d}{dt}\left(\frac{\partial KE}{\partial \dot{q}_i}\right) - \frac{\partial KE}{\partial q_i} + \frac{\partial PE}{\partial q_i} + \frac{\partial DE}{\partial \dot{q}_i} = \tau_i \qquad (i = 1, 2, ...n) \tag{6}$$

which is the Lagrange-Euler equation. In this expression *KE* and *PE* are the kinetic energy and potential energy of the system, respectively, *DE* is the dissipa-

tion energy, τ_i represents the generalized forces and torques at joint *i,* and q_i is the *i*th generalized coordinate. Dissipation energy *DE* may be neglected in the absence of damping.

After the application of Eq. (6) the dynamic equation of the robot can be obtained in matrix form as

$$\mathbf{D}(q)\,\ddot{q} + \mathbf{c}(q, \dot{q}) + \mathbf{h}(q) + \mathbf{b}(\dot{q}) = \tau \tag{7}$$

Equation (7) is a set of coupled and nonlinear second-order differential equations, the parameters of which are functions of the instantaneous state-space configuration of the robot. More specifically, [**D**(*q*] is called the manipulator inertia tensor[14]. The elements of this matrix can be given as[12]:

$$D_{ik} = \sum_{j=\max(i,k)}^{n} Tr(\mathbf{U}_{jk}\mathbf{I}_j\mathbf{U}_{ji}^T) \qquad i,k = 1,2,\ ...,\ n \tag{8}$$

c(**q, $\dot{\mathbf{q}}$**) is the n × 1 velocity coupling vector that expresses nonlinear Coriolis and centrifugal forces. The elements of this vector can be expressed as:

$$\mathbf{c}(q, \dot{q}) = (c_1\ c_2\ ...\ c_n)^T$$

where

$$C_i = \sum_{k=1}^{n}\sum_{m=1}^{n}\sum_{j=\max(i,k,m)}^{n} Tr(\mathbf{U}_{jkm}\mathbf{I}_j\mathbf{U}_{ji}^T)\dot{q}_k\dot{q}_m \qquad i,k,m = 1,2,...,m \tag{9}$$

h(**q**) in Eq. (7) is the gravity loading vector. The elements of the **h**(**q**) vector can be expressed as

$$\mathbf{h}(q) = (h_1 h_2 ... h_n)^T$$

where $$h_i = \sum_{j=1}^{n}(-m_j\mathbf{g}\mathbf{U}_{ji}\mathbf{r}_j^i) \qquad i = 1,2,\ ...,\ n \tag{10}$$

b($\dot{q}$) is the torque due to frictional forces. Friction will be neglected in the current study.

In the above expressions

$\mathbf{I}_i$ is the mass moment of inertia of link *i*

g is the gravity vector, and

$$\mathbf{U}_{kj} = \begin{cases} \mathbf{T}_0^{k-1}\,\mathbf{Q}_j\,\mathbf{T}_{j-2}^{k} & \text{for } j \le k \\ 0 & \text{for } j > k \end{cases}$$

and $$\mathbf{U}_{kjl} \equiv \frac{\partial \mathbf{U}_{kj}}{\partial q_i} \equiv \begin{cases} \mathbf{T}_0^{j-1}\mathbf{Q}_j\mathbf{T}_{j-1}^{l-1}\mathbf{Q}_k\mathbf{T}_{l-1}^{k} & i \geq k \geq j \\ \mathbf{T}_0^{l-1}\mathbf{Q}_l\mathbf{T}_{l-1}^{j-1}\mathbf{Q}_j\mathbf{T}_{j-1}^{k} & k \geq j \geq l \\ 0 & k < k \ \ or \ \ \mathrm{k} < l \end{cases}$$

where $$\mathbf{T}_{k-1}^{k} = \begin{bmatrix} C\theta_k & -C\alpha_k S\theta_k & S\alpha_k S\theta_k & \alpha_k C\theta_k \\ S\theta_k & C\alpha_k C\theta_k & -S\alpha_k C\theta_k & \alpha_k S\theta_k \\ 0 & S\alpha_k & C\alpha_k & d_k \\ 0 & 0 & 0 & 1 \end{bmatrix}$$

which is the homogeneous coordinate transformation matrix. In the latter matrix

$C\theta_k = \cos\,\theta_k$,

and

$S\theta_k = \sin\,\theta_k$,

a_k, d_k and α_k are kinematic parameters for link k.

These general relationships, when applied to the three-link robot of Fig. 4, can be simplified to the form

$$\begin{bmatrix} D_{11} & D_{12} & D_{13} \\ D_{12} & D_{22} & D_{23} \\ D_{13} & D_{23} & D_{33} \end{bmatrix} \begin{bmatrix} \ddot{\theta}_1 \\ \ddot{\theta}_2 \\ \ddot{\theta}_3 \end{bmatrix} + \begin{bmatrix} c_1(\theta_i, \dot{\theta}_i) \\ c_2(\theta_i, \dot{\theta}_i) \\ c_3(\theta_i, \dot{\theta}_i) \end{bmatrix} + \begin{bmatrix} h_1(\theta_i) \\ h_2(\theta_i) \\ h_3(\theta_i) \end{bmatrix} = \begin{bmatrix} \tau_1 \\ \tau_2 \\ \tau_3 \end{bmatrix} \quad i = 1,2,3 \qquad (11)$$

where the vector $[\tau_1 \ \ \tau_2 \ \ \tau_3]^T$ represents the torque vector.

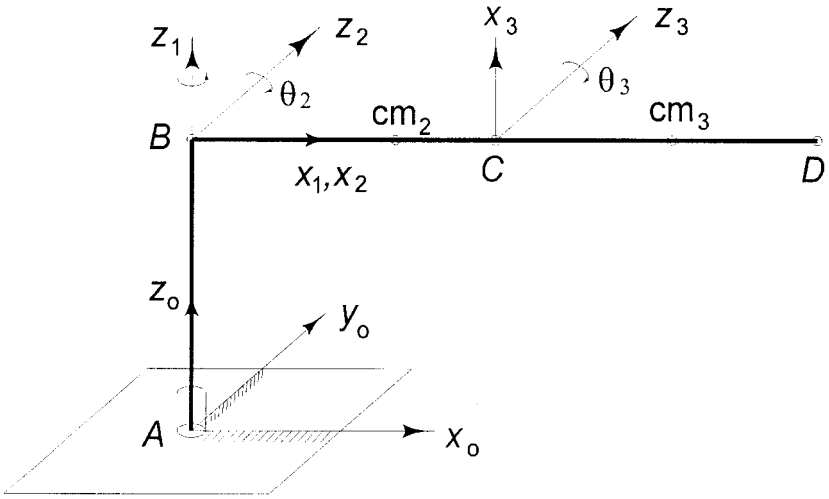

FIG. 4. Nomenclature for the KAU robot.

Aljawi[13] developed programs for the automatic generation of the complex, highly coupled non-linear second-order differential equations related to Equation[11]. These involved inertia loadings, coupled reaction forces (centrifugal and Coriolis) between joints, and the gravitational loading effects. The relevant expressions were expounded in algebraic form by the use of a symbolic computer algebra language package (Maple V). Appendix A presents these expressions for elements D_{11} to D_{33}, c_1 to c_3, and h_1 to h_3 after simplification by a set of assumptions.

In an effort to demonstrate the application of Eq. (11) to a practical design situation, the values listed in Appendix B were utilized. These masses, moments of inertia, distances and dimensions belong to the KAU robot[10,12,13]. It was assumed that the robot is programmed such that, while moving from an initial coordinate toward a point of destination, accelerations and decelerations vary in a cycloidal fashion, *i.e.,* the trajectory is a straight-line connection between two Cartesian points in space, and the time function for the trajectory is cycloidal:

$$\begin{bmatrix} x_i \\ y_i \\ z_i \end{bmatrix} = \begin{bmatrix} x_1 \\ y_2 \\ z_3 \end{bmatrix} + \lambda(t) \begin{bmatrix} x_2 - x_1 \\ y_2 - y_1 \\ z_2 - z_1 \end{bmatrix}$$

$$\text{where} \quad \lambda(t) = \frac{t}{t_f} - \frac{1}{2\pi} \text{ Sin } 2\pi \frac{t}{t_f} \qquad 0 \le t \le t_f$$

Figure 5a shows the variation of angular displacements at joints located at *A, B* and *C* (Fig. 4) as point *D* is moved from an initial location of [1, 0.1, 0.1] meters to a final destination of [0.1, 1, 1] meters during 2.0 seconds. Point *D* is raised up by about 0.9 m while the robot rotates. Thus θ_1 starts from about 4º, and rotates tawafwise (in the direction of circumambulation about the Kaaba) about 80º. Arm *BC* is practically horizontal at the beginning of the motion, and starts ascending until it stabilizes at about $\theta_2 = -50º$. The forearm (member *CD*) starts from a negative inclination of about $\theta_3 = 30º$, rises to above 10º, and then descends to about – 38º. Figures 5b and 5c illustrate the variation of the angular velocities (thetad 1, 2, and 3) and angular accelerations (thetad 1, 2 and 3) during the same motion. The smoothering effect of cycloidal motion is clearly visible in the latter curves.

Figure 5d shows the variation of torques at the three joints during the same motion. It may be verified by comparison of the acceleration curves of Fig. 5c and the torque curves of Fig. 5d that the latter look like exaggerated forms of the former. This observation is especially clear for joints 1 and 2. The maximum torque requirement of about 47 N-m occurs at joint *B* during this motion,

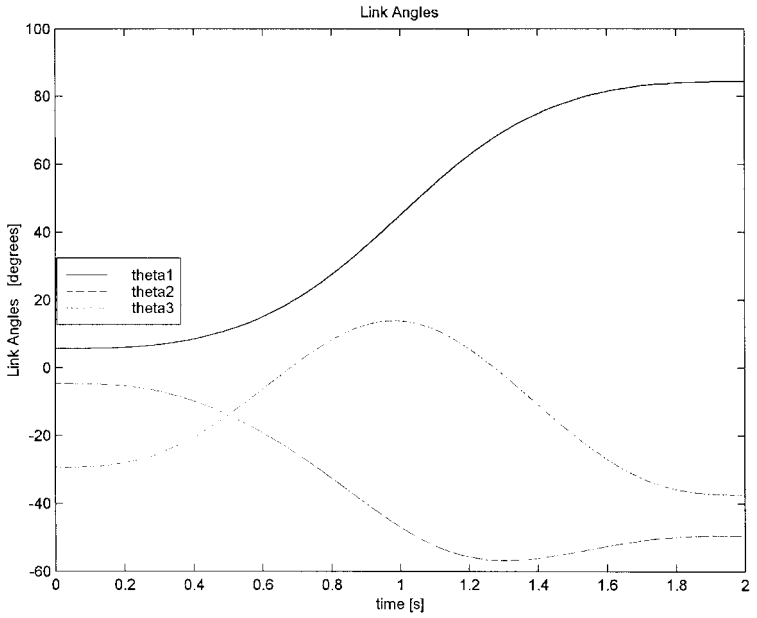
Link Angles
Link Angles [degrees]
time [s]
theta1
theta2
theta3
100
80
60
40
20
0
-20
-40
-60
0
0.2
0.4
0.6
0.8
1
1.2
1.4
1.6
1.8
2

(a)

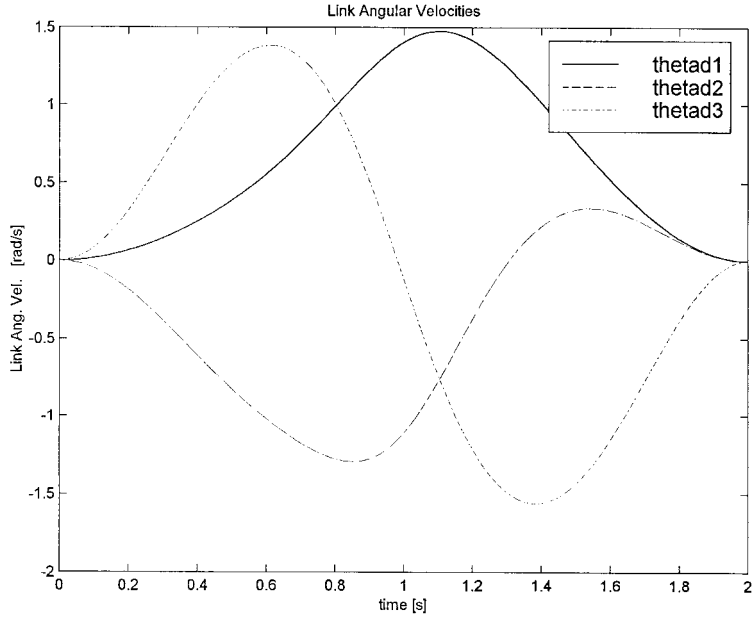
Link Angular Velocities
Link Ang. Vel. [rad/s]
time [s]
thetad1
thetad2
thetad3
1.5
1
0.5
0
-0.5
-1
-1.5
-2
0
0.2
0.4
0.6
0.8
1
1.2
1.4
1.6
1.8
2

(b)

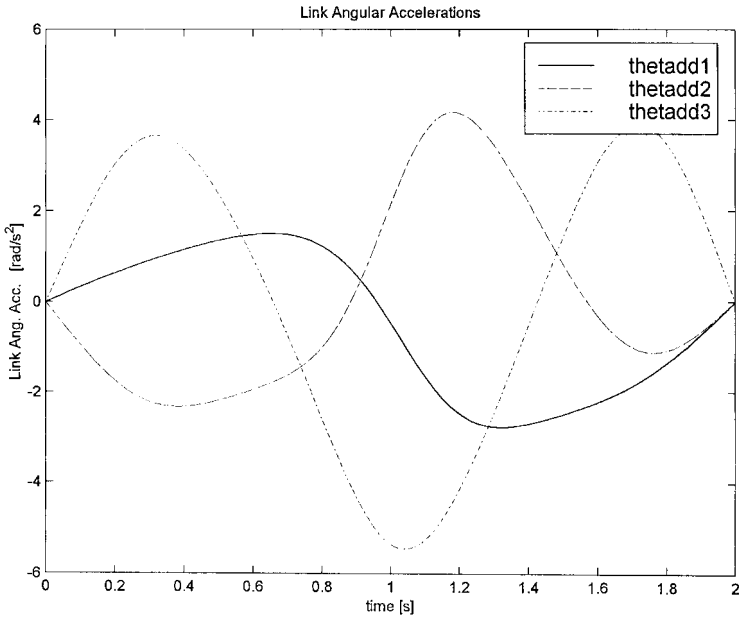

(c)

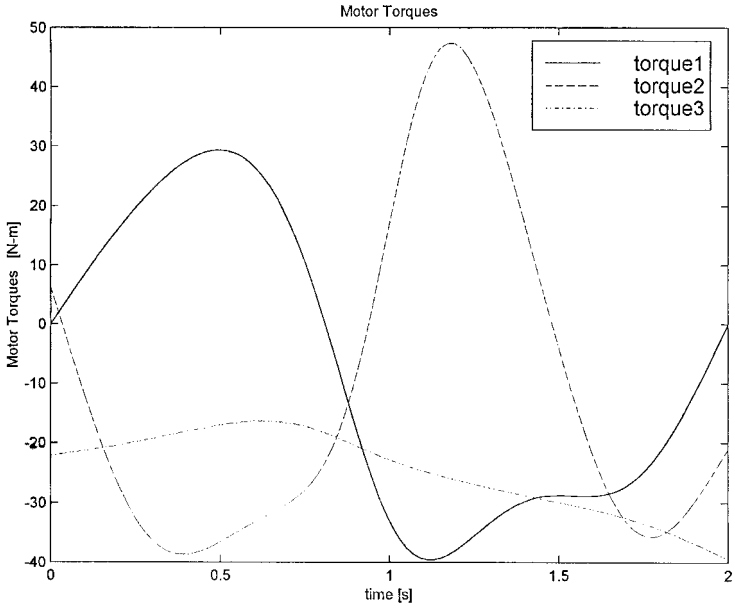

(d)

FIG. 5. Kinematic and dynamic output for the KAU robot.

followed by a torque of about –39 N-m at both joints *A* and *C*. The comparatively modest torque requirement at joint *B* may be attributed to the presence of a counter weight on member *BC*. It may be also noted in this connection that the center of mass on member *CD* has been adjusted by design to be situated close to point *C* (Appendix B).

Figure 6 shows the variation of torques at joints *A, B* and *C* (Fig. 4) as point *D* is lowered from an initial location of [0.1, 1] meters to a final destination of [1, 0.1, 0.1] meters during 2.0 seconds. Point *D* is lowered by about 0.9 m while the robot rotates clockwise by about 80º. This motion may be viewed as the opposite of that depicted in Fig. 5. It would be expected hence, that the torque curves of Fig. 6 be the mirror image (about the vertical axis) of those displayed in Fig. 5d. It may be verified from a study of these figures that this indeed is the case.

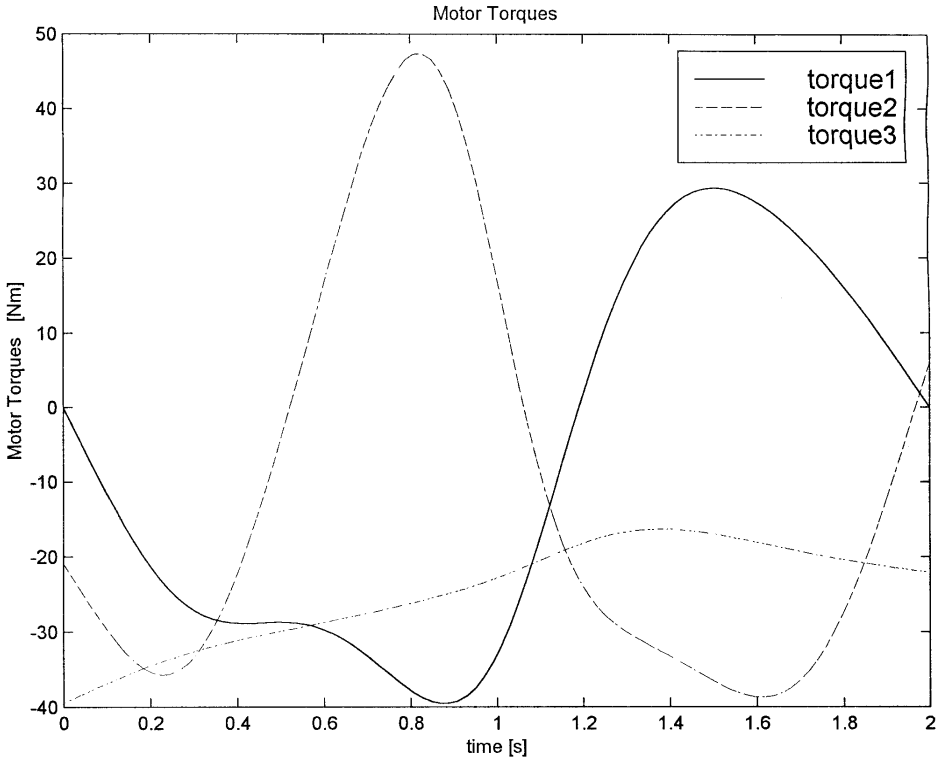

FIG. 6. Torque requirements for reverse motion.

It would be interesting to study the effect of the duration of a given motion, in terms of time, on torque requirements. To this end, the robot was programmed to execute the same motion, *i.e.,* to point *D* was lowered from an ini-

tial location at [0.1, 1, 1] meters to a final destination of [1, 0.1, 0.1] meters during a period of one second, and then to travel the same path during 4 seconds. Figure 7 shows the variation of torque requirements during the 4-second motion, and Fig. 8 for the one-second motion.

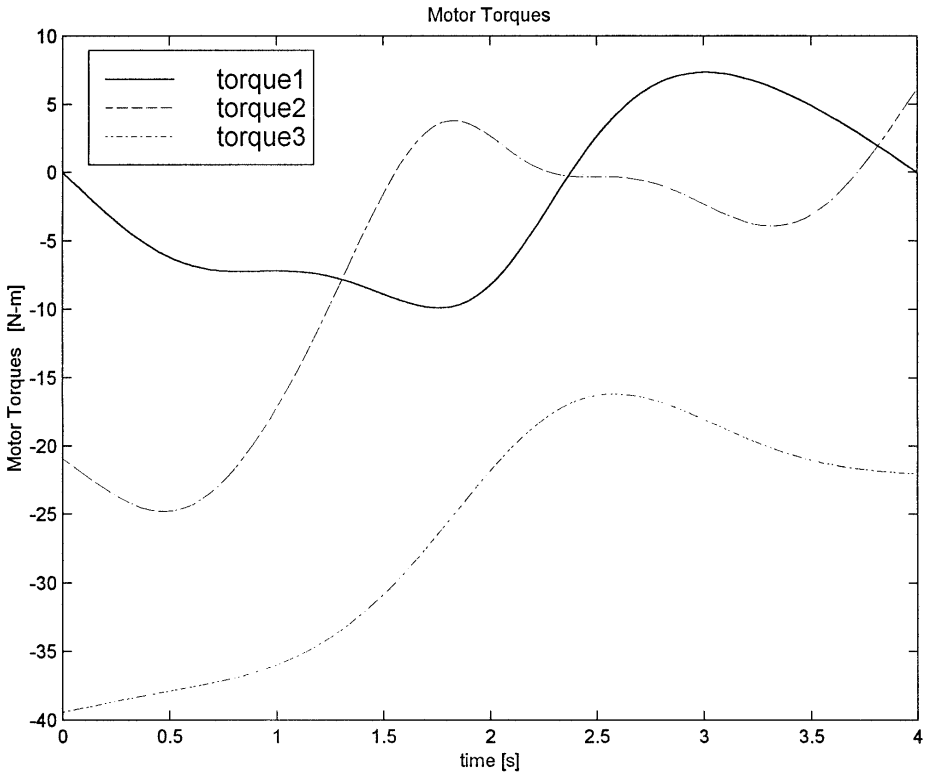

FIG. 7. Variation of torque requirements for a motion lasting 4 seconds.

It may be observed from Fig. 7 that the maximum positive torque requirement of about 7 N-m occurs at joint *A*. A negative torque value in excess of 35 N-m is observed at the start of the motion at point *C*. This torque shrinks in value to about –15 N-m near mid-motion. A comparison of Fig. 7 and Fig. 6 shows that the two sets of curves are similar in nature, as may be expected, but that the curves in Fig. 7 are smaller in amplitude at joints *A* and *B*. Torque requirements at joint *C* are found to be essentially the same in both graphs.

The shapes of the torque at joints *A* and *B* are strikingly similar in Figs. 6 and 8, the only difference being in amplitude. To cite an example, the largest torque requirement of about 225 N-m occurs at joint *B* (Fig. 8) for a period of one second. This is to be compared with a torque of 47 N-m that occurs for a period of

2 seconds. The sharp increases in the peaks of torque at *A* and *B* may be attributed to the relatively large inertia values for members *AB* and *BC*. The phenomenon of amplification in magnitude is not noticed for the torque requirement at joint *C* when the period of motion is shortened, although a slight depression is noticed at mid-cycle (Fig. 8).

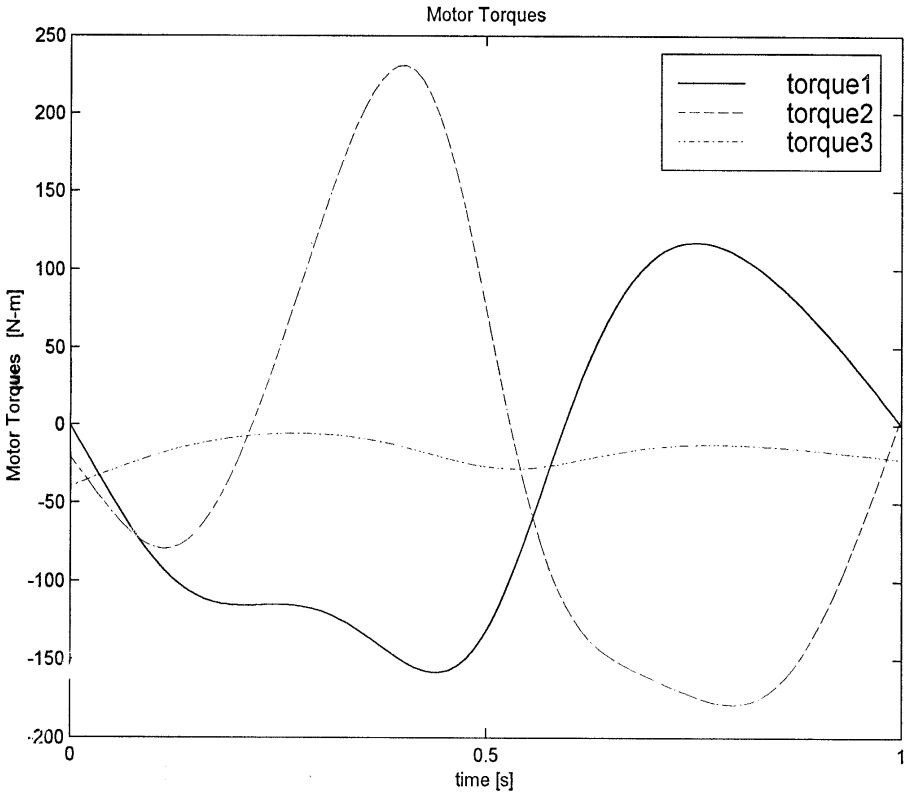

FIG. 8. Variation of torque requirements for the same motion lasting one second.

4. Concluding Remarks

It may be concluded, from the discussion on angular velocities, that angular velocities in the three-link arm tend to remain generally below 3 rad/s for a weighted tip velocity of unity per second. It is noted that magnitudes of the required angular velocities are dependent on *b,* generally growing with it. The practical and realistic example depicted in Fig. 5b for the case of the KAU robot may be cited for reinforcing the predictions on angular velocities. In the latter case, the value of *b* is 0.7, and the magnitudes of all angular velocities are observed to remain below 2 rad/s throughout the motion.

The general equations of motion for a robot were simplified during the current study, and adapted to the special case of the three-link KAU robot. The complex and highly coupled non-linear second-order differential equations involving inertial loadings, coupled reaction forces (centrifugal and Coriolis) between joints, and the gravitational loading effects were processed as a part of the effort.

In order to demonstrate the application of these relationships to a practical design situation, the actual magnitudes and values for the KAAU robot were utilized. It was assumed that the robot is programmed such that, while moving from an initial coordinate toward a point of destination, accelerations and decelerations vary in a cycloidal fashion. The results from the torque analysis clearly demonstrate the dominating effect of the period of motion on the torque requirements at each joint.

It may be concluded that the tools of analysis developed during the current study may be of utility during the design and development of new robots, or the improvement of performance of existing ones. The availability of such tools helps delineate the torque requirements at each axis of a given robot design, and hence assists in validating the choices for servomotors and gearheads that are needed to drive the robot for performing pre-defined tasks.

Acknowledgment

This work was partially sponsored by King Abdulaziz City for Science and Technology, Riyadh, through grant no. AR-12-42.

References

[1] **Groover, M.P., Weiss, M., Nagel, R.N.** and **Odrey, N.G.,** *Industrial Robotics: Technology, Programming, and Applications,* McGraw-Hill, 1986.

[2] **Mannaa, A.R., Dehlawi, F.** and **Akyurt, M.,** Geometric design considerations for a 3-link robot arm, *Computers in Industry,* **7,5,** 395-400, 1986.

[3] **Raghavan, M., Mehta, S.I., Pathre, U.** and **Vaishampayan, K.V.,** Mechanical design of an industrial robot, *Indian J Technol.,* v **24** n 3, March 1986, p. 149.

[4] **Herbest, L.,** Robot specification tradeoffs for specific applications, *Proc. Robot 8 Conf.,* June 1984, p. 16-1.

[5] **Kim, Jin-Oh,** Task-based Kinematic Design of Robot Manipulators, *Ph.D. Thesis, Carnegie Mellon University,* 1992, 180 p.

[6] **Park, C.,** The Optimal Design of Mechanisms, *Ph.D. Thesis, Harvard University,* 1991, 103 p.

[7] **Yoshimura, M.,** Design optimization of industrial robots considering the working environment, *Int J Prod Res,* v **28** n 5, May 1990, 805-820.

[8] **Kravchenko, N.F.,** Assessment of the effect of quasi-inertia & quasi-force additions when designing an industrial robot, *Sov Eng Res,* **9,** 12, 1989, 9-11.

[9] **Husain, M., Malik, A.** and **Ghosh, A.,** Design improvement of manipulators by minimizing shaking force/moment & driving torques, *Proc. 22nd Biennial Mechanisms Conf., ASME,* 1992, 139-147.

[10] **Akyurt, M., Balamesh, A.S., Aljawi, A.A.N.** and **Dehlawi, F.M.A.,** On the synthesis of articulated robotic arms, *J. Isl. Acad. Sci.* (Accepted, 5/99).
[11] **Klafter, R.D., Chmielewski, T.A.** and **Negin, M.,** *Robotic Engineering: an Integrated Approach,* Prentice-Hall, 1989.
[12] **Balamesh, A.S.** and **Aljawi, A.A.A.,** "Robsim: A Robot Motion Simulator on MATLAB, *"Proc. 5th Saudi Eng. Conf., February 1999,* Umm Al-Qura Univ., Makkah, v **4,** pp. 419-427, 1999.
[13] **Aljawi, A.A.N.,** Symbolic Formulation of Dynamic Equations for KAU Robotic Manipulators, *Technical Journal, Univ. Eng. Tech., Taxila,* pp. 1-12, 1999.
[14] **Schilling, R.J.,** *Fundamentals of Robotics, Analysis and Control,* Prentice Hall, 1990.

Appendix A

Elements of the Matrices of Equation 11

$$h_1 := 0$$

$$h_2 := -4.905\, m2\, 11\cos(\theta_2) + 4.905\, m3\sin(\theta_2)\, 12\sin(\theta_3) - 4.905\, m3\cos(\theta_2)\, 12\cos(\theta_3) - 9.81\, m3\, 11\cos(\theta_2)$$

$$h_3 := 4.905\, m3\sin(\theta_2)\, 12\sin(\theta_3) - 4.905\, m3\cos(\theta_2)\, 12\cos(\theta_3)$$

$$D_{11} := \frac{1}{2} Jx_2 \%2 + Jx_1 + mx_3\, 11\cos(\theta_3) + m3\, al^2 + m2\, al^2 - my_3 11\sin(\theta_3) + Jz_1 + \frac{1}{2} m2\, 11^2 + mx_3\, 12 - my_3\, 12\sin(\%1) + \frac{1}{2} m3\, 11^2 + \frac{1}{2} m3\, 12^2 + \frac{1}{2} m2\, 11^2\, \%2 - \frac{1}{2} Jy_3\cos(\%1) + mx_2 11 + mx_2\, 11\%2 + \frac{1}{2} m3\ 11^2\, \%2 + \frac{1}{2} Jx_3\cos(\%1) - my_2 11\sin(2\theta_2) + mx_3\, 12\cos(\%1) - my_3\, 11\sin(\theta_3 + 2\theta_2) + mx_3\, 11\cos(\theta_3 + 2\theta_2) - \frac{1}{2} Jy_2 \%2 + \frac{1}{2} Jy_2 + \frac{1}{2} Jx_2 + Jz_2 + \frac{1}{2} Jy_3 + \frac{1}{2} Jx_3 + Jz_3 + m3\, 12\, 11\cos(\theta_3 + 2\theta_2) + \frac{1}{2} m3\ 12^2\cos(\%1) + m3\, 12\cos(\theta_3)\, 11$$

$$\%1 := 2\theta_3 + 2\theta_2$$

$$\%2 := \cos(2\theta_2)$$

$$D_{12} := \cos(\theta_2)\, my_2\ al + \sin(\theta_2)\, mx_2\ al + 11\sin(\theta_2)\, m2\ al + my_3\ al\cos(\theta_2 + \theta_3) + m3\, 12\ al\sin(\theta_2 + \theta_3) + mx_3\ al\sin(\theta_2 + \theta_3) + m3\, 11\sin(\theta_2)\, al$$

$$D_{13} := mx_3\ al\sin(\theta_2 + \theta_3) + my_3\ al\cos(\theta_2 + \theta_3) + m3\, 12\ al\sin(\theta_2 + \theta_3)$$

$$D_{22} := 2mx_3\, 11\cos(\theta_3) - 2my_3\, 11\sin(\theta_3) + m2\, 11^2 + 2\ mx_3\, 12 + m3\ 11^2 + m3\ 12^2 + 2\ mx_2\, 11 + Jy_2 + Jx_2 + Jy_3 + Jx_3 + 2m3\ 12\cos(\theta_3)\, 11$$

$$D_{23} := mx_3\, 11\cos(\theta_3) - my_3 11\sin(\theta_3) + 2\ mx_3\, 12 + m3\, 12^2 + Jy_3 + Jx_3 + m3\, 12\cos(\theta_3)\, 11$$

$$D_{21} = D_{12}$$

$$D_{31} = D_{13}$$

$$D_{32} = D_{23}$$

$$D_{33} := 2\ mx_3 12 + m3\ 12^2 + Jy_3 + Jx_3$$

$$\begin{aligned} C_1 := \; & -v1\ v2\ m3\ \ 11^2\ \%2 - 2\ v1\ v2\ my_3\ 11\cos(\%4) - v1\ v3\ m3\ 11\ 12\ \sin(\theta_3) \\ & - 2\ v1\ v2\ my_3\ 12\ \cos(\%1) - v1\ v3\ m3\ \ 11\ \ 12\ \sin(\%4) + v1\ v3\ Jy_3\ \sin(\%1) \\ & - v3^2\ my_3\ al\ \sin(\%3) + v3^2\ m3\ 12\ al\ \cos(\%3) - v1\ v3\ my_3\ \cos(\theta_3)\ 11 \\ & + v3^2\ mx_3\ al\ \cos(\%3) - 2\ v1\ v3\ mx_3\ 12\ \sin(\%1) - v2^2\ \ my_3\ al\ in(\%3) \\ & + v2^2\ \ mx_3\ el\ \cos(\%3) + 2\ v2\ v3\ mx_3\ al\ \cos(\%3) - 2\ v1\ v2\ m3\ 12\ 11\ \sin(\%4) \\ & - 2\ v2\ v3\ my_3\ al\ \sin(\%3) - 2\ v1\ v2\ 11\ my_2\ \cos(2\theta_2) + v1\ v2\ Jy_2\ \%2 \\ & - v1\ v3\ mx_3\ 11\ \sin(\%4) + 2\ v2\ v3\ m3\ 12\ al\ \cos(\%3) - 2\ v1\ v3\ my_3\ 12\ \cos(\%1) \\ & - v1\ v3\ my_3\ 11\ \cos(\%4) + v2^2\ 11\ \cos(\theta_2)\ m2\ al + v2^2\ \ m3\ 11\ \cos(\theta_2)\ al \\ & + v2^2\ \cos(\theta_2)\ mx_2\ \ al - v2^2\ \sin(\theta_2)\ my_2\ \ al - v1\ v2\ m3\ 12^2\ \ \sin(\%1) \\ & - v1\ v3\ mx_3\ 11\ \sin(\theta_3) - v1\ v3\ m3\ 12^2\ \sin(\%1) - v1\ v3\ Jx_3\ \sin(\%1) \\ & + v1\ v2\ \ Jy_3\ \sin(\%1) - v1\ v2\ \ Jx_3\ \sin(\%1) - 2\ v1\ v2\ mx_3\ 11\ \sin(\%4) \\ & + v2^2\ m3\ 12\ \ al\ \cos(\%3) - 2\ v1\ v2\ 11\ mx_2\ \ \%2 - v1\ v2\ 11^2\ \ m2\ \%2 - v1\ v2\ \ Kx_2\ \ \%2 \\ & - 2\ v1\ v2\ mx_3\ 12\ \sin(\%1) \end{aligned}$$

$$\%1 := 2\theta_3 + 2\theta_2$$

$$\%2 := \sin(2\theta_2)$$

$$\%3 := \theta_2 + \theta_3$$

$$\%4 := \theta_3 + \theta_2$$

$$\begin{aligned} C_2 := \; & v1^2\ mx_3\ 12\ \sin(\%2) + v1^2\ \ mx_3\ 11\ \sin(\theta_3 + 2\theta_2) + v1^2\ \ 11\ mx_2\ \ \%1 \\ & - \frac{1}{2}\ v1^2\ \ Jy_3\ \ \sin(\%2) + \frac{1}{2}\ v1^2\ \ Jx_3\ \sin(\%2) - 2\ v3\ 11\ v2\ \ m3\ 12\ \sin(\theta_3) \\ & - 2\ v3\ 11\ v2\ \ my_3\ \cos(\theta_3) - v3^2\ \ m3\ 11\ 12\ \sin(\theta_3) - v3^2\ \ my_3\ 11\ \cos(\theta_3) \\ & - 2\ v3\ 11\ v2\ \ mx_3\ \sin(\theta_3) - v3^2\ \ mx_3\ 11\ \sin(\theta_3) + v1^2\ \ my_3\ 12\ \cos(\%2) \\ & + \frac{1}{2}\ v1^2\ m3\ 11^2\ \ \%1 + \frac{1}{2}\ vl^2\ m3\ 12^2\ \ \sin(\%2) + vl^2\ \ 11\ my_2\ \ \cos(2\theta_2) \\ & + \frac{1}{2}\ v1^2\ \ 11^2\ \ m2\ \%1 + v1^2\ \ my_3\ 11\ \cos(\theta_3 + 2\theta_2) + v1^2\ \ m3\ 12\ 11\ \sin(\theta_3 + 2\theta_2) \\ & + \frac{1}{2}\ v1^2\ \ Jx_2\ \ \%1\ \ - \frac{1}{2}\ v1^2\ \ Jy_2\ \%1 \end{aligned}$$

$$\%1 := \sin(2\theta_2)$$

$$\%2 := 2\theta_3 + 2\theta$$

$$C_3 := v1^2\ mx_3\ 12\sin(\%1) + \frac{1}{2} v1^2\ \ mx_3\ 11\sin(\theta_3 + 2\theta_2) + v2^2\ 11\, my_3\cos(\theta_3)$$

$$+ v2^2\ 11\, m3\, 12\sin(\theta_3) + v2^2\ 11\, mx_3\sin(\theta_3) - \frac{1}{2} v1^2\ Jy_3\sin(\%1)$$

$$+ \frac{1}{2} v1^2\ Jx_3\sin(\%1) + \frac{1}{2} v1^2\ m3\, 11\, 12\sin(\theta_3) + \frac{1}{2} v1^2\ mx_3\, 11\sin(\theta_3)$$

$$+ \frac{1}{2} v1^2\, my_3\, 11\cos(\theta_3) + v1^2\ my_3\, 12\cos(\%1) + \frac{1}{2} v1^2\, m3\, 12^2\sin(\%1)$$

$$+ \frac{1}{2} v1^2\ my_3\, 11\cos(\theta_3 + 2\theta_2) + \frac{1}{2} v1^2\ m3\, 12\, 11\sin(\theta_3 + 2\theta_2)$$

$$\%1 := 2\theta_3 + 2\theta_2$$

Appendix B

Magnitudes for the KAU Robot

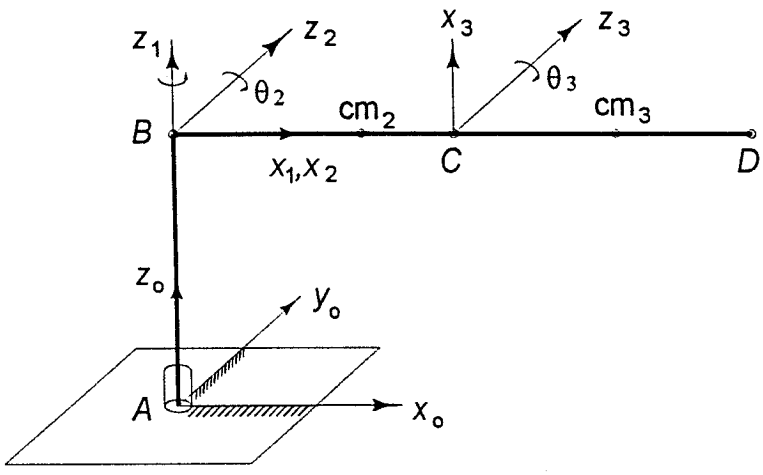

AB = 0.50 m

BC = 0.70 m

CD = 0.55 m

$I_{zz1} = 0.926$ kg-m^2

$I_{zz2} = 8.19$ kg-m^2 $\quad I_{yy2} = 7.97$ kg-m^2

$I_{zz3} = 0.512$ kg-m^2 $\quad I_{zz3} = 0.54$ kg-m^2

$m_1 = 57.5$ kg

$m_2 = 66.1$ kg $\quad cm_2 = -0.24$ m

$m_3 = 10.9$ kg $\quad cm_3 = -0.009$ m

concentrated mass at D = 7.50 kg

متطلبـــات القـــدرة لـذراع روبـــوتي مفصـــــلي

عبد الغفار أزهري نواوي الجاوي ، مهمت أكيورت
حمزة دايكن ، هيثم بوقس و فؤاد دهلوي
كلية الهندسة ، جامعة الملك عبد العزيز
جـــــدة – المملكة العربية السعودية

المستخلص . لقد تم النظر في متطلبات السرعة الزاويّة والعزم لذراع روبوتي مفصلي مكون من تجميع ثلاث وصلات وثلاثة مفاصل دوّارة للتحقق من تأثير أطوال الوصلات على متطلبات السرعة الزاويّة . فقد تم تأسيس وتوضيح العلاقة الكينماتية لحركة السطوح الموجهة لسرعات طرفية مختارة . وعلاوة على ذلك تم عرض المعادلات العامة لتحديد متطلبات العزم عند وصلات الذراع . وقد تم تطبيق النتائج على مواصفات الحركة لمجموعة روبوت مختارة .